ONLINE DETERMINATION OF NOISE LEVEL IN WEATHER RADARS

Igor R. Ivić[(1)(2)], and Sebastian M. Torres[(1)(2)]

(1) Cooperative Institute for Mesoscale Meteorological Studies (CIMMS), The University of Oklahoma
(2) NOAA/OAR National Severe Storms Laboratory, Norman, Oklahoma

1. INTRODUCTION

Proper measurement of noise power is of paramount importance for the estimation and quality control (a.k.a. censoring) of the weather radar data, which, in turn, is essential for the correct operation of automated algorithms and accurate forecasts derived from such data.

Incorrect noise power measurements may lead to reduction of coverage in cases where the noise power is overestimated or to radar data images cluttered by speckles if the noise power is underestimated. Consequently, correct noise power measurement is essential for proper operation of censoring techniques in both single and dual-polarized radars (Ivić and Torres 2009, Ivić et al. 2009). Moreover, if erroneous noise power is used at low signal-to-noise ratios (SNR), estimators tend to produce biased meteorological variables (i.e., reflectivity and spectrum width as well as differential reflectivity and cross-correlation coefficient in case of dual-polarized radars).

Typically, the noise power in weather radars can be measured in several ways. For instance, on the National Weather Surveillance Radar – 1988 Doppler (WSR-88D) the noise measurement is part of the online system calibrations performed after each volume scan. Such measurement takes place at a high antenna elevation angle and the result is adjusted using predetermined correction factors for other antenna elevations. In systems that do not have the capability to perform online calibrations (e.g., the National Weather Radar Testbed Phased-Array Radar) the noise power must be measured offline. Evidently, the downside of such approach is that it does not capture the temporal variations of noise power. Moreover, the nature of the noise sources in radar data is such that the noise power can have angular dependence in both azimuth and elevation (e.g., noise from cosmic radiation and from the oxygen and water vapor molecules) (Doviak and Zrnić 1993). Consequently, the benefit of noise measurements at each antenna position becomes obvious. The only way such measurement can be performed operationally is in parallel with data collection. Thus, an efficient approach that estimates noise power from measurements that contain both signal and noise is desirable.

Ideally, noise power estimates would be produced at every sampling volume (e.g., by using spectral noise estimation methods). In the past, several techniques have been proposed. Hildebrand and Sekhon (1974) described a method that subjects the Fourier coefficients to a series of tests whereby coefficients are

recursively discarded until statistical conditions suggest only noise samples remain. Urkowitz and Nespor (1992) used the Kolmogorov-Smirnov (K-S) test applied to the periodogram by successively discarding the Fourier spectral lines until the criterion for the noise hypothesis is satisfied. Siggia and Passarelli (2004) used rank order statistics on power spectral density estimates to dynamically determine the noise level. Common to these approaches is discarding excess Fourier coefficients until the remaining ones satisfy conditions for noise. Inevitably, each approach introduces bias in noise level determination even if no signal is present and particularly for radar volumes with weather signals that have wide spectrum widths or if using a small number of samples in the dwell time. This cannot be avoided and the only question is how significant the bias is.

Ivić and Torres (2010) proposed a technique that performs more precise and continuous system noise power calibration. This technique is robust and feasible for real-time implementation on weather radars. The proposed method estimates the system noise power dynamically from the in-phase and quadrature data components at every antenna position (radial). The technique uses a novel criterion to detect radar volumes that do not contain significant weather signals and the system noise power from samples at these locations. Because it does not use the Fourier coefficients, this method overcomes the limitations of spectral-processing-based techniques in cases when the numbers of samples at each range volume is small. This is usually the case in the so called surveillance mode where the unambiguous range is long and the number of range volumes devoid of signal is more than sufficient for accurate noise estimation.

In this work an improvement to the technique proposed by Ivić and Torres (2010) is presented. The number of steps in the procedure is reduced making it significantly simpler. Also, no prior knowledge of the approximate noise power is needed (unlike with the previously proposed method). The improved technique is evaluated on time-series collected with the National Weather Radar Testbed Phased-Array Radar (NWRT PAR) (Zrnić et. al. 2007), located in Norman, OK. Results show that the proposed technique produces noise power estimates that are closely matched to the ones obtained from manually identified, signal-free radar volumes at far ranges from the radar; thus, providing empirical validation.

2. NOISE POWER ESTIMATION ALGORITHM

Unlike the single-volume methods proposed by other authors, the algorithm presented in this paper produces a common noise power estimate for all radar volumes at the same antenna position (or radial) by using data from range volumes in which the presence of

Corresponding author address: Igor R. Ivić, CIMMS/NSSL, 120 David L. Boren Blvd., Norman, OK 73072; email: Igor.Ivic@noaa.gov

signal is not detected. The assumption is that there are enough range volumes devoid of signal to yield noise power estimates with satisfactory accuracy. This is almost always true when using long pulse repetition times (PRT), which result in unambiguous ranges in excess of 300 km. On the other hand, when the PRT yields shorter unambiguous ranges, it is possible that the majority of samples contain signal as storms span or exceed the entire unambiguous range. In such cases, the algorithm is unable to produce reliable noise power estimates. For dual PRT scans (i.e., those using a long PRT for range coverage and a short PRT for Doppler velocity measurements), if the noise power at a given antenna position cannot be estimated from the short PRT data, it is usually available from the long PRT data.

To illustrate the steps of the noise estimation algorithm we will use data collected with the NWRT PAR. This particular set of data was collected in a long PRT mode with unambiguous range of 465.6 km, which is typically used at low elevation angles. Radar echoes are range oversampled by a factor of 4; i.e., samples are 60 m apart and the transmitted pulse is roughly 240 m long. The number of samples (M) in the dwell time is 15, which results in dwell times typical of operational scanning strategies. This radar does not perform online calibrations so the default noise level is measured offline. The test power profile is shown in Figure 1. By visual inspection, we notice that the power is rather flat and weak beyond the 5000-th sample. This indicates that there should be no signal present at those ranges. By averaging the power of all samples beyond 5000, 5500, and 6000 we get 18.106, 17.65 and 17.6. Thus, we assume the "true" noise power to be 17.6 (12.46 dB) in this case.
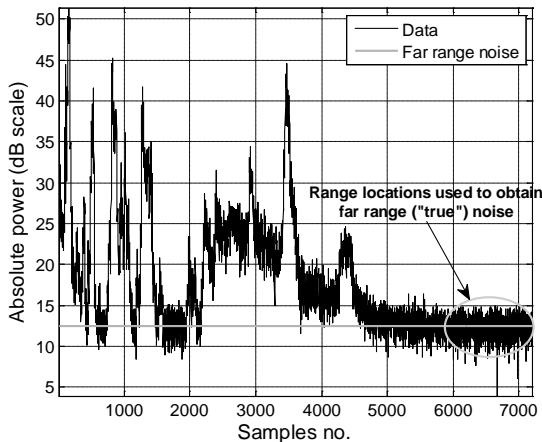
Figure 1. Received power as a function of range at the elevation angle of 0.5 deg. The number of samples for each radar volume is 15 and the range sample spacing is 60 m. The "true" noise power is indicated with a grey line. This data was collected using the NWRT PAR in Norman, OK.

In the first step of the algorithm the portions of power profile with flat power are identified as this is an indication of the potential signal-free regions. This is done by estimating the local variance of powers at each range location from K samples as

$$Var_{dB}(k) = \sum_{n=k}^{k+K-1} \left(\hat{P}_{dB}(n) - \frac{1}{K} \sum_{l=k}^{k+K-1} \hat{P}_{dB}(l) \right)^2$$
$$= \sum_{n=k}^{k+K-1} \left(10\log_{10} \left(\frac{\hat{P}(n)}{\prod_{l=k}^{k+K-1} \hat{P}(l)^{1/K}} \right) \right)^2, \quad (1)$$

where

$$\hat{P}(k) = \frac{1}{M} \sum_{m=0}^{M-1} |V(m,k)|^2,$$
$$\hat{P}_{dB}(k) = 10\log_{10} \left(\frac{1}{M} \sum_{m=0}^{M-1} |V(m,k)|^2 \right) = 10\log_{10}\left(\hat{P}(k)\right). \quad (2)$$

and $V(m,k)$ is the m-th sample at a range location k. The value of (1) can be used as an indication of signal presence. To illustrate this, time-series containing noise and signal+noise, with SNR linearly increasing from 0 to 5 dB for K values of 50, 100 and 150, were generated and histograms showing probability density functions (pdfs) for $Var_{dB}(k)$ are presented in Figure 2. As expected, the amount of overlap between noise and signal+noise pdfs is inversely proportional to K. Other aspect, which should be taken into consideration, is that if K is too large then the shorter flat areas, in the SNR profile, can easily pass undetected which can cause algorithm to fail due to insufficient amount of data. This becomes more important when using non-oversampled data and/or when the PRT is short. Consequently, the parameter K is chosen to be 150 in further discussion.
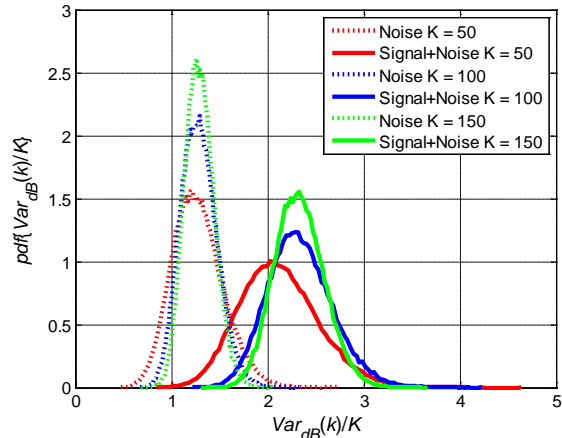

Figure 2. Histograms of local variance for different numbers of samples.

Clearly, a threshold needs to be set such that any local variance estimate larger than some value is classified as "signal-like". There are two aspects to choosing this threshold. If it is chosen too high, then too many samples containing signal will be classified as noise. On the other hand, if the threshold is chosen too low, excessive number of noise only samples are discarded, and the resulting noise estimate may be significantly biased. We choose to set the threshold THR so that

$$\int_{THR}^{\infty} pdf_{Var_{dB}(k)}(x)\,dx = 0.01\,. \qquad (3)$$

Because variance is estimated from powers in logarithmic units, the threshold value is not dependent on the absolute value of the noise power in the system. Another advantage of this approach is that the power estimates in logarithmic units are part of the reflectivity calculations, so the amount of additional computations incurred by the procedure is minimized. In particular, if M is 15 and K is 150 the threshold is 252. The results of applying this threshold are shown in Figure 3 where areas classified as noise only are highlighted in grey. Note that the power profile has been normalized by the far range (i.e., 'true') noise power to obtain SNR. It is apparent that areas which contain strong signal, but are rather flat, are classified as potential noise by this step; thus, if retained, these samples can severely bias the noise estimate. Consequently, further filtering is needed.
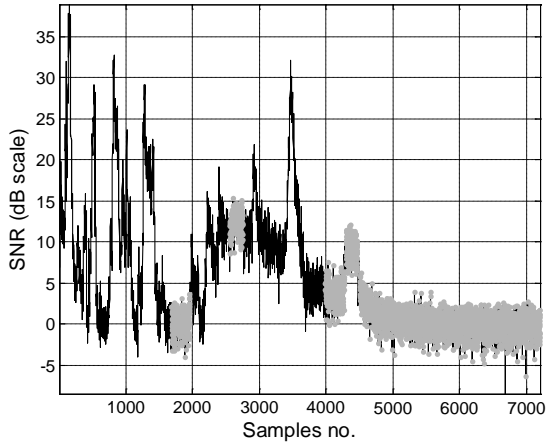
Figure 3. SNR profile with regions selected as potential noise, in the first algorithm step, highlighted in grey.
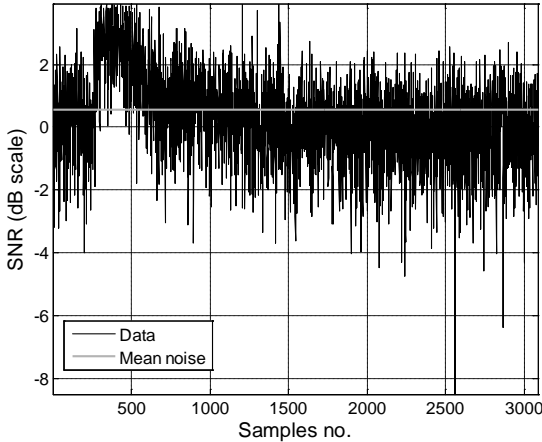

Figure 4. SNR profile of data after discarding samples at regions where power is larger than THR_{int}.

Next, the mean power is calculated for each set of contiguous range locations classified as noise. Out of these estimates the smallest one is taken to be the intermediate noise estimate (N_{int}). Then, we discard all samples at range locations for which power estimate is
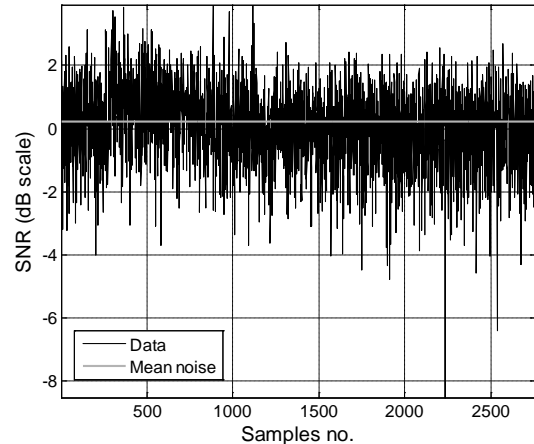
larger than the threshold THR_{int} chosen as (Appendix A in Ivić 2009)

$$\Gamma_{inc}\left(THR_{int}\,\frac{M}{N_{int}},M\right) = 10^{-5}\,. \qquad (4)$$

In this particular case, M is 15 and the THR_{int} equals $2.5N_{int}$. The power profile of the remaining data is given in Figure 4 and the mean power is 0.552 dB above the far range noise.
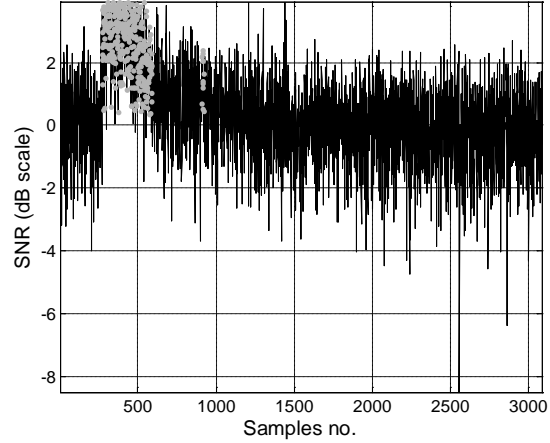
(a)

(b)

Figure 5. (a) Highlighted range locations discarded by the range 'persistence' filter. (b) SNR profile after data at highlighted locations has been removed.

The next step is to apply a "range persistence" filter. The filter finds 10 or more consecutive power values that are larger than the median power in the set and discards them along with 10 samples on either side. The rationale for choosing 10 consecutive samples is following. The probability that one power sample is larger than the median is 0.5; hence, the probability that 10 randomly chosen independent samples are larger than the median is $0.5^{10} = 9.76 \times 10^{-4}$. Consequently, this filter should detect and remove larger sample powers (evidence of signal-like returns) that exhibit some continuity in range while leaving those in predominantly noise areas. Range locations that are discarded by the range persistence filter are highlighted in Figure 5a.

After these are removed, we obtain Figure 5b. The mean power of the resulting set is 0.23 dB higher than the "true" noise power for this case.

In the third step, the matrix of samples (range time vs. sample time) is reshaped into a vector where the samples from 1 to M belong to the first column of the matrix, samples M+1 to $2M$ belong to the second column of the matrix and so on. Then, a running average of K samples is performed as

$$RAVG(m-K) = \frac{1}{K}\sum_{k=0}^{K-1}|V(m-k)|^2, \quad m \geq K \quad (5)$$

where $V(k)$ are the elements of the reshaped samples vector. K needs to be large enough to make the remaining weak signal detectable and is chosen to be 750. Figure 6 shows the power profile resulting from applying the moving average on the sample data set. Note that this makes the SNR range profile of (5) appear higher in the region encompassing samples 3000 to 13000 which is an indication of signal presence. In a noise-only case, the probability that one averaged point is larger than the mean N times D is (Ivić and Zrnić 2009)

$$\frac{K}{N \cdot (K-1)!}\int_{D \cdot N}^{\infty}\left(\frac{K}{N}p\right)^{K-1}e^{-p\frac{K}{N}}dp = \Gamma_{inc}(D \cdot K, K) \quad (6)$$

When D is 1.1 (or 110% of the mean noise power) and K is 750, this probability is 0.38%. The mean is found from the data after the range persistence filter. Averaged points that are larger by more than 10% of the so found mean (herein referred to as "outliers") are detected and all samples that went into the averaged points are discarded. This is repeated while the number of discarded samples is larger than 0.0038 times the total number of samples or up to a maximum of five iterations. In this particular case the outlier filtering is performed three times. Data discarded in the first iteration is grayed in Figure 6. The mean power after the last step is 17.61, which is in almost perfect agreement with the "true" or far range noise level.
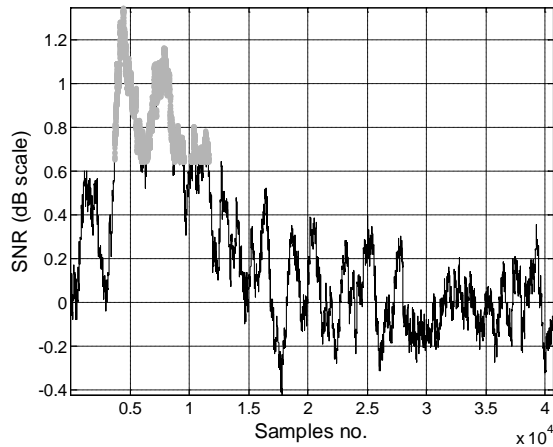
Figure 6. Power range profile after applying moving average filter with positions discarded in the first iteration of the algorithm highlighted in grey.

The steps of the algorithm are summarized below:

1) *Calculate variance as given by* (1) *and classify each range position as either containing signal, or not, by comparing to a threshold.*

2) *Group consecutive range locations, classified as signal free, and estimate mean power for each group. Take the smallest estimate and calculate the threshold based on it so it satisfies* (4) *(e.g., using Newton iteration).*

3) *Run range persistence filter that detects 10 or more consecutive samples with power larger than the median and discard them plus 10 surrounding samples on each side.*

4) *Reshape all samples into a one dimensional array.*

5) *Obtain mean power.*

6) *Perform running average of 750 points.*

7) *Discard samples used to obtain averaged points larger than 1.1 times the mean power from step 5.*

8) *If the number of discarded samples is smaller than 0.0038 times the total number of samples or the number of repetitions of steps 5, 6, and 7 is 5, exit algorithm and output power obtained in step 5. Otherwise, go back to step 5.*

3. PERFORMANCE EXAMPLES

In this section, two examples of the algorithm performance on time-series data are presented. Both sets of data were collected with the NWRT PAR. As mentioned before, this radar does not perform online calibrations; thus, if noise is not estimated from data, the initial value of 19.5 (obtained by offline measurements) is used for product generation. The first data set is from a dual PRT tilt with a long PRT of 3.104 ms and the number of samples (M) is 15. A short PRT is 0.896 ms, with M of 44, at an elevation of 0.51 deg. The algorithm is set so that if fewer than 1000 samples remain after step 8, the technique is unable to produce a reliable noise power estimate. By imposing the requirement that the estimates are made from at least 1000 samples, the algorithm is prevented from producing results when the majority of samples contain signal. Additionally, if exactly 1000 samples are used for estimation, the estimate is within ±10% of the true mean with 0.998 probability. In this particular example, the algorithm fails to produce results from the short PRT data rather often. When this occurs, the one from the long PRT is used. In this example however, even in the cases when the algorithm produces results from the short PRT data, the samples are usually heavily inundated with signal so the noise power is frequently overestimated. Consequently, the short-PRT and long-PRT estimates are compared and the two results are combined only if they are within 5% of each other. Otherwise, only the long PRT estimate is used. In Figure 7a, the estimated noise power is plotted with the one obtained from the distant ranges free of visible signals (the "true" noise). This shows that the proposed noise power estimator is reliable and robust as it produces values close to the true noise power. Figure 7b shows the reflectivity field
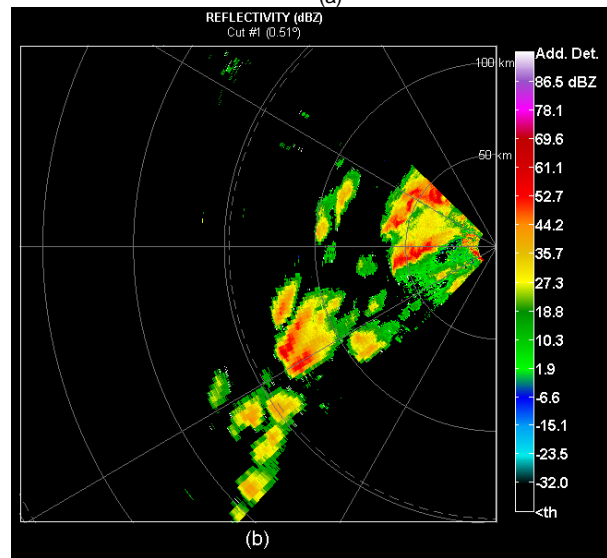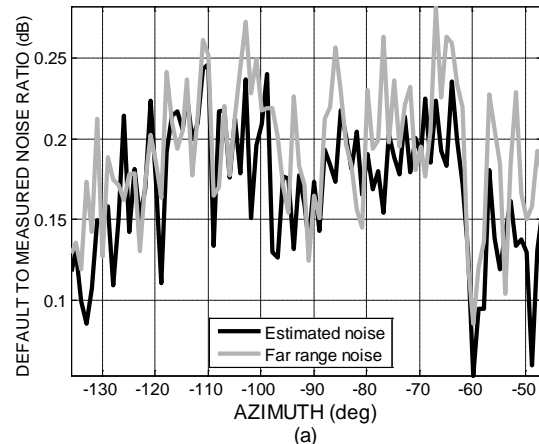
obtained using the estimated noise power and using CBT (Coherency Based Thresholding) for detection (Ivić and Torres 2009). The additional detections obtained using the estimated noise power as opposed to the default one are highlighted in white. Total number of detections is 50335 if using the default noise and the additional 1527 (3% more) are gained when using the noise estimation technique.

(a)

(b)
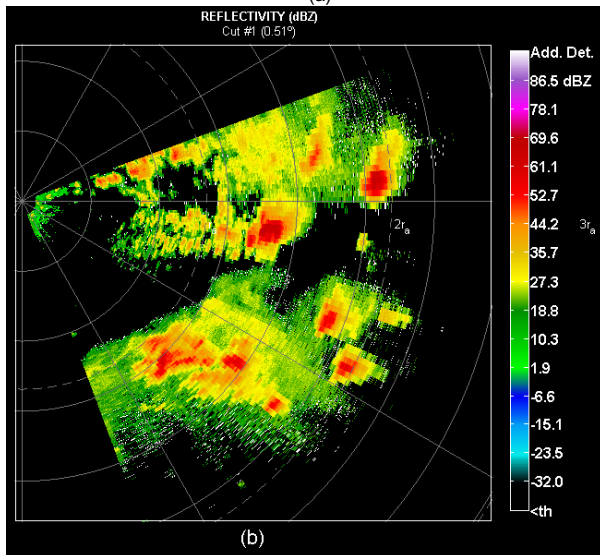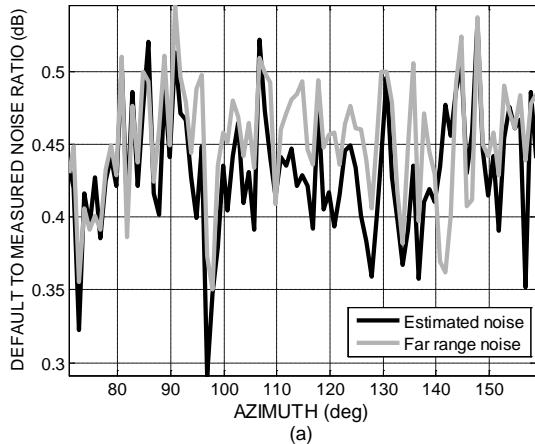
Figure 7. (a) Noise estimates compared to the initial (default) and the far range ("true") noise, and (b) reflectivity field with additional detections obtained using estimated noise highlighted in white.

Another example is presented next. The PRT used for this scan was 3.104 ms with 15 samples ($M = 15$) per dwell for surveillance and 44 pulses at 0.984 ms for Doppler scan. The results are presented in Figure 8. As in the previous case, it is apparent, from Figure 8a, that the estimated and the "true" noises agree very well. Figure 8b shows the reflectivity field obtained using the coherency based censoring technique (CBT). Additional detections resulted from the use of the noise power estimation algorithm are highlighted in white. In this particular case, these are minimal because the default noise power is, on average, only 0.16 dB above the

estimated one. Consequently, additional detections account for only 178 out of 27057 (or 0.7%).

(a)

(b)

Figure 8. (a) Noise estimates compared to the initial (default) and the far range ("true") noise, and (b) reflectivity field with additional detections obtained using estimated noise highlighted in white.

4. SUMMARY

A method to estimate noise power dynamically from data was presented. Through a set of steps, the algorithm classifies samples as containing signal or not. The main advantage of this technique is that it does not require an initial rough guess on the noise power. First, running local variance is calculated for the power data and it is compared to a predetermined threshold. This detects areas of the range profile that are rather flat as this is an indication of potential signal-free locations. For each group of consecutive range locations that are classified as potentially signal-free, the mean power is estimated. Based on the smallest value, another threshold is produced so that range locations with power larger than this threshold are discarded and new data set is obtained. Then, range locations with powers that are consecutively higher than the median are removed. At this point, all the remaining samples are rearranged into a row vector and a running average is performed to

make the remaining weak signal areas more evident. To dispense with the remaining signal, all samples associated with the averaged points larger than 10% of the mean power are discarded. The last step is repeated until the fraction of discarded samples falls under 0.0038. The noise estimate is produced from the remaining samples by finding mean power. In the implementation presented in this paper, the minimum number of the remaining samples required to produce reliable estimate is set to be 1000. The algorithm accuracy was verified by comparing its results to the noise powers obtained from the data at the far range positions devoid of visible signals. Such comparison shows that the technique produces noise powers with improved accuracy as opposed to offline and online calibrations with minimal bias.

REFERENCES

Doviak, R.J., and D.S. Zrnić, 1993: *Doppler radar and weather observations*. Academic Press, 562 pp.

Hildebrand P. H., and R. S. Sekhon, 1974: Objective Determination of the Noise Level in Doppler Spectra, *Journal of Applied Meteorology*, **13**, 808-811.

Ivić I. R., *Detection Threshold for Spectral Moments and Polarimetric Variables*. Saarbrücken: VDM Verlag Dr. Müller AG & Co., 2009, pp. 199.

Ivić I. R., and S. M. Torres, 2009: Using Signal Coherency to Improve Detection on Weather Radars, *34th Conference on Radar Meteorology*, Williamsburg, VA, AMS.

Ivić I. R., and S. M. Torres, 2010: Online Determination of Noise Level in Weather Radars, *ERAD 2010*, Sibiu, Romania.

Siggia A. D., and R.E. Passarelli, 2004: Gaussian Model Adaptive Processing (GMAP) for Improved Ground Clutter Cancellation and Moment Calculation, *ERAD 2004*, Visby, Sweden, 67-73.

Urkowitz H., and J. D. Nespor, 1992: Obtaining Spectral Moments by Discrete Fourier Transform with Noise Removal in Radar Meteorology, *Int. Geoscience and Remote Sensing Symp.,* Houston, TX, IGARSS, 125–127.

Zrnić, D. S., J. F. Kimpel, D. E. Forsyth, A. Shapiro, G. Crain, R. Ferek, J. Heimmer, W. Benner, T.J. McNellis, R.J. Vogt, 2007: Agile beam phased array radar for weather observations. *Bull. Amer. Meteor. Soc.*, **88**, 1753-1766

Zrnić D.S., 1975: Simulation of weather like Doppler spectra and signals, *J. Appl. Meteorol.*, 619-620.

APPENDIX A

In this appendix, we derive the expression for threshold used in the first step of the algorithm. To do this we need to know the *pdf* of $Var_{dB}(k)$ in case all samples are white noise. Because $Var_{dB}(k)$ is function of numerous random variables the analytical derivation of the *pdf* using variable transformation becomes intractable. One solution would be to find threshold through search using Monte-Carlo simulations (Zrnić 1975). Even with such an approach it would be beneficial to have an analytical expression which could produce approximate threshold value which would then be corrected using simulations. The *pdf* shapes in Figure 2 are similar to the gamma distribution:

$$f(x) = \begin{cases} \dfrac{x^{\alpha-1}e^{-x/\theta}}{\theta^\alpha \Gamma(\alpha)} & \text{if } x > 0 \\ 0 & \text{if } x < 0 \end{cases}. \qquad (A.1)$$

This distribution is defined by the first two moments; thus, if we analytically derive the first two moments of the $Var_{dB}(k)$ estimator we can produce the *pdf* model to be used in the search. We start by deriving the first moment as

$$E\{\hat{V}ar_{dB}(k)\} = E\left\{ \sum_{n=k}^{k+K-1}\left(\hat{P}_{dB}(n) - \frac{1}{K}\sum_{l=k}^{k+K-1}\hat{P}_{dB}(l)\right)^2 \right\} \\ = (K-1)\left(E\{\hat{P}_{dB}^2(k)\} - E^2\{\hat{P}_{dB}(k)\}\right). \qquad (A.2)$$

Hence, to calculate the terms in (A.2) we need to derive the *pdf* of

$$\hat{P}_{dB}(k) = 10\log_{10}\left(\frac{1}{M}\sum_{m=0}^{M-1}|V(m,k)|^2\right) = 10\log_{10}\left(\hat{P}(k)\right) \quad (A.3)$$

We do this using the known *pdf* of $\hat{P}(k)$ from Ivić (2009) and get

$$f_{\hat{P}_{dB}(k)}(y) = \frac{\ln 10}{10}M^M 10^{\frac{y}{10}M}\frac{e^{-\frac{M}{N}10^{\frac{y}{10}}}}{N^M(M-1)!}. \qquad (A.4)$$

So now,

$$\sum_{n=k}^{k+K-1}E\{\hat{P}_{dB}^k(n)\} = \frac{KM^M \ln 10}{10N^M(M-1)!}\int_0^\infty y^k 10^{\frac{y}{10}M}e^{-\frac{M}{N}10^{\frac{y}{10}}}dy. \quad (A.5)$$

which we can evaluate numerically. Next, we find the second moment as

$$E\{Var_{dB}^2(k)\} = E\left\{\left(\sum_{n=k}^{k+K-1}\hat{P}_{dB}^2(n)\right)^2\right\} + \\ E\left\{\left(\sum_{n=k}^{k+K-1}\hat{P}_{dB}^2(n)\right)^4\right\} + \\ 2\left(1-\frac{2}{K}\right)E\left\{\sum_{n=k}^{k+K-1}\hat{P}_{dB}^2(n)\left(\sum_{l=k}^{k+K-1}\hat{P}_{dB}(l)\right)^2\right\}$$

$$= E\left\{\hat{P}_{dB}^4(0)\right\}\left(K-2+\frac{1}{K}\right)+$$

$$E^2\left\{\hat{P}_{dB}^2(0)\right\}\left(K^2-3K+5-\frac{3}{K}\right)+$$

$$E\left\{\hat{P}_{dB}^2(0)\right\}E^2\left\{\hat{P}_{dB}(0)\right\}\times$$

$$\frac{-2K^3+12K^2-22K+12}{K}+ \qquad\text{(A.6)}$$

$$4E\left\{\hat{P}_{dB}(0)\right\}E\left\{\hat{P}_{dB}^3(0)\right\}\left(2-K-\frac{1}{K}\right)+$$

$$\frac{(K-1)(K-2)(K-3)}{K}E^4\left\{\hat{P}_{dB}(0)\right\}$$

We can check how well the gamma distribution models the *pdf* of $Var_{dB}(k)$ by comparing the third and the fourth moment obtained using Monte-Carlo simulations and those calculated as

$$E\left\{Var_{dB}^n(k)\right\}=\prod_{l=0}^{n-1}(\alpha+l)\theta^n , \qquad\text{(A.7)}$$

where

$$\alpha=\frac{E^2\left\{Var_{dB}(k)\right\}}{E\left\{Var_{dB}^2(k)\right\}-E^2\left\{Var_{dB}(k)\right\}},$$

$$\theta=\frac{E\left\{Var_{dB}^2(k)\right\}-E^2\left\{Var_{dB}(k)\right\}}{E\left\{Var_{dB}(k)\right\}}. \qquad\text{(A.8)}$$

This is shown in Figure 1.A. The plots imply that the gamma distribution matches the actual one up to the fourth moment.
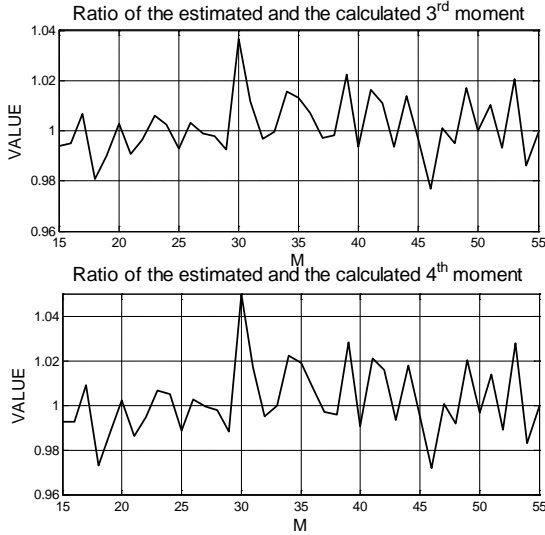
Figure 1.A. Ratio of the estimated and the calculated moments.

Accordingly, using a gamma distribution that satisfies (3) to produce the threshold should yield the desired result. This is presented in Fig. 2.A where the probability is estimated using plain Monte-Carlo integration as

$$\frac{1}{L}\sum_{l=0}^{L-1}D\left[Var_{dB}(l)>THR\right]. \qquad\text{(A.9)}$$

Using the gamma approximation, the threshold can be found using Newton iteration as

$$THR(n+1)=THR(n)+$$

$$\frac{\Gamma_{inc}\left(THR(n)\middle/\theta,\alpha\right)-0.01}{\left(THR(n)\middle/\theta\right)^{\alpha-1}\dfrac{\exp\left(THR(n)\middle/\theta\right)}{\Gamma(\alpha)}}, \qquad\text{(A.10)}$$

where

$$\Gamma(\alpha)=\int_0^\infty e^{-t}t^{\alpha-1}dt,\text{ and}$$

$$\Gamma_{inc}\left(\frac{THR(n)}{\theta},\alpha\right)=\frac{1}{\Gamma(\alpha)}\int_{THR(n)/\theta}^\infty e^{-t}t^{\alpha-1}dt, \qquad\text{(A.11)}$$

are gamma and gamma incomplete functions. The estimated probabilities presented in Figure 2.A imply that the threshold found using a gamma distribution produces the desired probabilities (0.01 in this case) up to the statistical error. Consequently, one can produce thresholds for each sample number (M) using a gamma distribution approximation and arrange those into table so they can be easily retrieved during real-time processing.
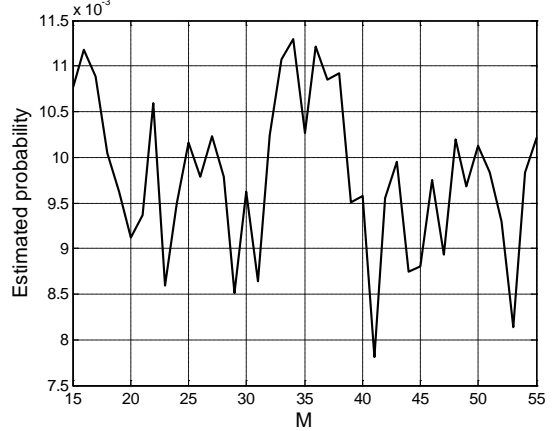
Figure 2.A. Probabilities obtained using Monte-Carlo integration with threshold assuming a gamma distribution.